

## Conference Proceeding

Paper presented at the 1st International Conference on Modern Technologies in Mechanical & Material Engineering [MTME 2023]

# A Comparative Analysis of the Influence of Welding Current on Microstructure and Mechanical Properties in TIG Welded Ti5Al2.5Sn Alloy

Aziz-ur-Rehman<sup>1</sup>, Fahd Nawaz Khan<sup>1</sup>, Huzaifa Asif<sup>1</sup>, Tauheed Shehbaz<sup>1\*</sup>, Balaji Aresh<sup>2</sup>

<sup>1</sup>Faculty of Materials and Chemical Engineering, Department of Materials Science, Ghulam Ishaq Khan Institute of Engineering Sciences and Technology, Topi 23640, Pakistan

<sup>2</sup>School of Computing, Engineering and Physical Sciences, University of West of Scotland (Paisley Campus), UK  
E-mail: tauheed@giki.edu.pk

**Received:** 25 May 2023; **Revised:** 30 June 2023; **Accepted:** 18 July 2023

**Abstract:** Tungsten inert gas (TIG) welding was performed on a 1.6 mm thick Ti5Al2.5Sn alloy sheet to analyze the influence of welding current on the resultant microstructure and mechanical properties in the weldments. Fusion zone (FZ) width was observed to increase with increasing the welding current. The heat-affected zone (HAZ) showed acicular  $\alpha$ , primary  $\alpha$  and  $\alpha'$  martensite phases depending upon the cooling rate. FZ was comprised of  $\alpha'$  martensite at the high cooling rate, acicular  $\alpha$  at a low cooling rate and some retained  $\beta$ . The ultimate tensile strength (UTS), notch tensile strength (NTS) and impact toughness in all the weldments increased from 754 MPa to 810 MPa, 703 MPa to 785 MPa, and 2.3 J to 3.3 J, respectively, by increasing the welding current. However, percentage elongation decreased from 10% to 6.5% by increasing the welding current from 12 A to 18 A. Moreover, the impact toughness value was observed to increase by increasing welding current owing to the formation of a higher proportion in acicular  $\alpha$ ,  $\alpha'$  martensite phases within the FZ. Furthermore, higher microhardness was achieved at higher currents.

**Keywords:** TIG welding, microstructure, titanium alloy, mechanical properties

## Nomenclature

BM	Base metal
EDM	Electric discharge machining
EDXS	Energy-dispersive X-ray spectroscopy
FZ	Fusion zone
HAZ	Heat-affected zone
LBW	Laser beam welding
Nd: YAG	Neodymium-doped yttrium aluminium garnet
NTS	Notch tensile strength
TIG	Tungsten inert gas
UTS	Ultimate tensile strength

Copyright ©2023 Aziz-ur-Rehman, et al.  
DOI: <https://doi.org/10.37256/dmt.3220233093>  
This is an open-access article distributed under a CC BY license  
(Creative Commons Attribution 4.0 International License)  
<https://creativecommons.org/licenses/by/4.0/>

# 1. Introduction

Since titanium alloys are low density and have high specific strength, biocompatibility, and corrosion resistance, they find most applications in the automotive and aerospace industries [1-3]. Titanium alloys have also been used widely in chemical processing, sports components, and marine applications [4]. Ti5Al2.5Sn has superior creep properties compared to Ti6Al4V and titanium alloys [5-7]. Welding is the most prevalent process for producing complicated structural elements made of titanium alloys [8]. Welding can be performed in several ways such as the laser, electron beam, and argon gas arc welding [9-11]. As a result of its low assembly precision requirements, adaptability to non-linear welding, and general usefulness, argon arc welding has found widespread use in the aviation industry. Titanium alloys are mostly joined using a welding technique called TIG welding which is particularly useful when joining thin sheets of titanium [12-14].

Pulsed TIG welding refines the grain size, and increases the hardness, tensile strength and ductility [15]. The pulsed TIG welding technique was introduced in the 1950s. The high current value is adjusted to get penetration in weldments and the low current is adjusted to maintain arc stability. In this method of welding, heat dissipation is minimal so the width of HAZ is low.

In recent years, there has been a lot of attention and research on the microstructure of titanium and titanium TIG weldments. The mechanical properties and microstructures of TIG-welded commercially pure (CP) titanium were studied by Karpagaraj et al. [16]. They found that the FZ had a higher hardness than the starting alloy. Weld quality, mechanical properties, residual distortion, and microstructure were studied by Gao et al. [12] for joints made from Ti6Al4V alloy using Nd: YAG LBW and TIG welding. Microscopically, they found that the TIG welded joints' FZ had an acicular  $\alpha'$  morphology with secondary  $\alpha$  features. Tsai et al. [17] discovered TiAl +  $\alpha$ 2-Ti3Al formation in the FZ for the first time by studying the microstructural features of an investment cast Ti6Al4V.

For this study, we investigated the effects of varying the welding current while keeping all other variables constant during pulse TIG welding of the Ti5Al2.5Sn alloy sheet. For mechanical testing, tensile tests with both notch and smooth tensile samples were performed to check the strength of pulsed TIG weldments. An impact test was performed on impact (V-notched) samples to check the impact strength (impact toughness) of pulsed TIG welded samples. Microhardness distribution was measured throughout the morphology of metallographic samples from FZ to BM through the HAZ. For metallurgical characterization, optical microscopy was performed to observe different phases in all three zones (FZ, HAZ and BM). The present investigation is meant to contribute to a deeper understanding of the relationship between TIG welding current and the resulting welded joints' mechanical properties.

# 2. Materials and methods

In the present study, Ti5Al2.5Sn,  $\alpha$ -titanium alloy sheet was welded using Miller (XMT 456 CC/CV) Pulsed TIG welding. The dimensions of the sheet used were 100 × 75 × 1.6 mm. Analysis of chemical composition was measured by using EDXS as presented in Table 1.

**Table 1.** EDXS analysis of the chemical composition of Ti5Al2.5Sn in wt.%

Ti	Al	Sn	Mo	V	O	Si	Fe	C	N
Balance	5.34	2.56	< 0.01	0.02	0.17	0.03	0.27	0.01	0.01

A micro pulsed-TIG welding machine (Micro Pulse-300, Precision System, UK) was used for the welding process. Argon was used as a shielding gas to avoid the contamination of the titanium plate during the welding operation. To select the working ranges for important input parameters, many trials run (i.e., 8 times) were performed to obtain maximum weld pool depth and quality of the weld. After performing these trial runs, the optimum working parameters were obtained for the current study as shown in Table 2.

**Table 2.** Optimum parameters used for TIG welding

Current (A)	Welding speed (mm/min)	Voltage (V)	Arc length (mm)	Argon flow rate (L/min)
12	30	10	4	11.75
16	30	10	4	11.75
18	30	10	4	11.75

Optical microscopy was performed to study the different phases in FZ, HAZ, and BM. Wire-cutting EDM was used to prepare the metallographic, tensile and double-notch samples. Epoxy resin was used for the cold mounting of metallographic samples. After this, the samples were ground using SiC papers with grits ranging from 220 to 4000. In the end, polishing was performed using a polishing machine (Struers, Planopol-3). As an etchant, Kroll's reagent (92 ml of distilled water, 6 ml of HNO<sub>3</sub>, and 2 ml of HF) was used. For polarized microscopy, 2% HF solution was used as a second etchant after applying Kroll's solution.

Tensile testing was conducted using INSTRON-5567 universal testing machine at a constant strain rate of 2.5 mm/min. Smooth tensile samples were prepared as per ASTM E8M-04. The impact test was performed by using a Charpy impact testing machine (Brooks inspection equipment Ltd, Model: MAT21). The impact samples were prepared by making a 2 mm notch at one side of the weld centerline with an angle of 45°. The length, width, and thickness of impact samples were kept as 100 mm, 10 mm and 1.6 mm respectively. Microhardness measurement was performed using Wilson Tukon (Model: TU300 FM) tester. For this purpose, metallographic samples (cross-sectional) were used to study the hardness of FZ, HAZ and BM. A standard load of 200 gf was applied with 15 s dwell time.

### 3. Results and discussion

Physical appearance, optical microstructures and their relationship with mechanical properties are presented in this chapter

#### 3.1 Physical appearance

Figure 1 depicts the physical appearance of the top surface of each welded joint. The complete penetration weld joints were produced using the welding parameters as presented in Table 2. Furthermore, the presence of bluish appearance of the weldments indicates that the weldments were oxidized despite the usage of shielding gas during the welding process. This might be due to the insufficient shielding gas, or the coverage area of the shielding gas is inadequate, air can still reach the welding area and cause oxidation.

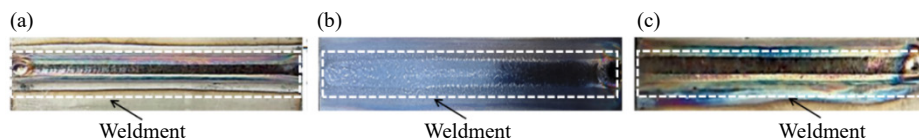


**Figure 1.** Topside images of the plates: (a) 12 A; (b) 16 A; (c) 18 A

#### 3.2 Microstructural analysis

An optical micrograph of the BM, Ti5Al2.5Sn, revealed that the matrix was composed of  $\alpha$  phase, with prior  $\beta$  phase at the grain boundaries. An average grain size of 40  $\mu\text{m}$  was measured using ImageJ software and is presented in Figure 2.

A significant difference was observed in the features of the HAZ/BM interface when the welding current was

increased from 12 to 18 A, at a constant welding speed of 30 mm/min. BM to HAZ grain size increased from 40  $\mu\text{m}$  to 480  $\mu\text{m}$ , 495  $\mu\text{m}$  and 510  $\mu\text{m}$  for welding currents of 12 A, 16 A and 18 A, respectively as seen in Figures 3(a), 3(b) and 3(c) as measured using ImageJ software. Moreover, the cooling rate is expected to be higher in HAZ near FZ as compared to that region of HAZ which was near BM, and hence the significant change in BM and HAZ microstructure. This can be due to the higher cooling rate in the HAZ near the FZ because the temperature in this region is closer to the melting point of the metal. As the metal solidifies, the rate of heat dissipation is higher in this region due to the larger temperature difference between the solidifying metal and the surrounding medium which results in a faster cooling rate.

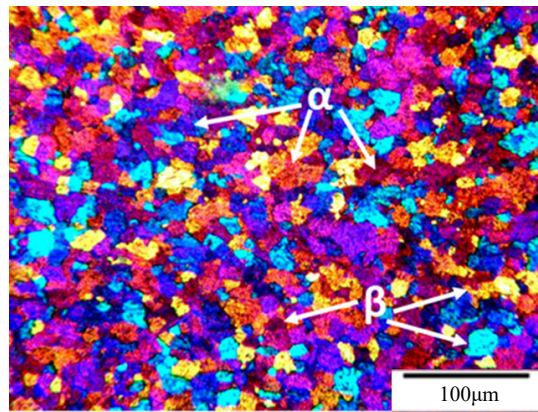


Figure 2. BM microstructure of Ti5Al2.5Sn

At higher welding currents, the grain size of all three weldments increased from the HAZ to the FZ. The complete refinement of grains in the FZ might be attributed to the  $\alpha'$  martensite phase, while the partial refinement of grains in the HAZ might be due to the presence of acicular  $\alpha$  and primary  $\alpha$  resulting in the formation of an equiaxed microstructure, as shown in Figure 3. Babu et al. [18] explained that a higher thermal gradient occurred which resulted in a non-uniform microstructure from the FZ to BM.

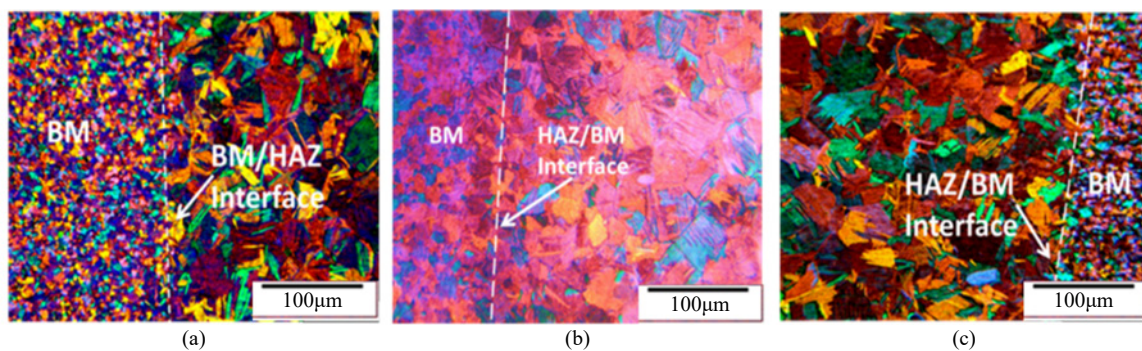


Figure 3. BM/HAZ interface at base currents: (a) 12 A; (b) 16 A; (c) 18 A

Columnar grains appeared in these microstructures, which may be attributed to the presence of martensite consisting of both  $\alpha'$  martensite and acicular  $\alpha$  as shown in Figure 3. Due to the pulsed TIG current, a refinement of grain size occurred, and the width of the HAZ decreased, as explained by both Babu et al. [18] and Balasubramanian et al. [19]. Gao et al. [12] explained that the region of HAZ near the BM is known as a partially transformed region which might be attributed to the presence of  $\alpha$  and  $\beta$  phases in HAZ. However, the region of HAZ near FZ is known as a fully transformed region owing to the transformation of primary  $\alpha$  or  $\beta$  phases. According to Akman et al. [20], HAZ may consist of  $\alpha'$  martensite, primary  $\alpha$ , and acicular  $\alpha$  depending upon the transformation from  $\beta$  phase at a particular

cooling rate.

At higher pulsed TIG welding current, the amount of  $\alpha'$  martensite in the FZ increased, which can be attributed to the high cooling rate resulting in a greater transformation. The FZ microstructures for pulsed TIG currents of 12 A, 16 A, and 18 A are shown in Figures 4(a), 4(b), and 4(c). The grains exhibited a columnar morphology, which may be attributed to the presence of  $\alpha'$  martensite at higher cooling rates and acicular  $\alpha$  at lower cooling rates, with some retained  $\beta$ . At higher magnifications, the columnar grains in the FZ showed clearer morphology, as observed in the HAZ region. Due to the pulsed current, refinement of the FZ occurred, which enhanced the mechanical properties, as explained by Balasubramanian et al. [19]. Moreover, high pulse frequency caused the molten pool to agitate which may increase the tensile strength [19]. Since  $\alpha$  titanium alloys have a low thermal conductivity, that means the cooling/solidification rate was slow thus, the grain size of FZ became larger as compared to HAZ [16].

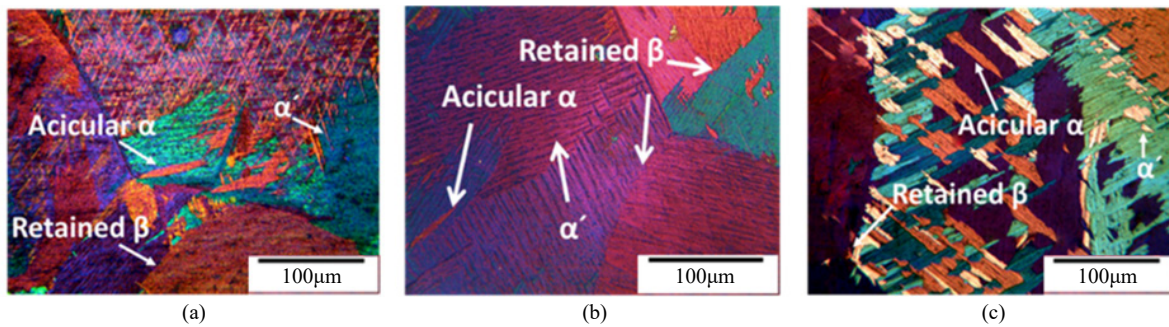


Figure 4. FZ microstructure at pulsed TIG welding current (Miller XMT 456 CC/CV): (a) 12 A; (b) 16 A; (c) 18 A

### 3.3 Microhardness analysis

At higher welding currents, an increase in microhardness was observed, which may be attributed to the increased heat input causing an increase in FZ oxidation. The microhardness distribution for welding current values of 12 A, 16 A, and 18 A is shown in Figure 5. The microhardness gradually decreased from the FZ to the BM through the HAZ in the order of FZ > HAZ > BM. This order of hardness may be justified by the formation of  $\alpha'$  martensite in the FZ for all the weldments, the presence of acicular  $\alpha$  and some retained  $\beta$  in the HAZ, and the presence of larger sizes of  $\alpha$  colonies and a smaller number of grain boundaries of  $\beta$  in the BM.

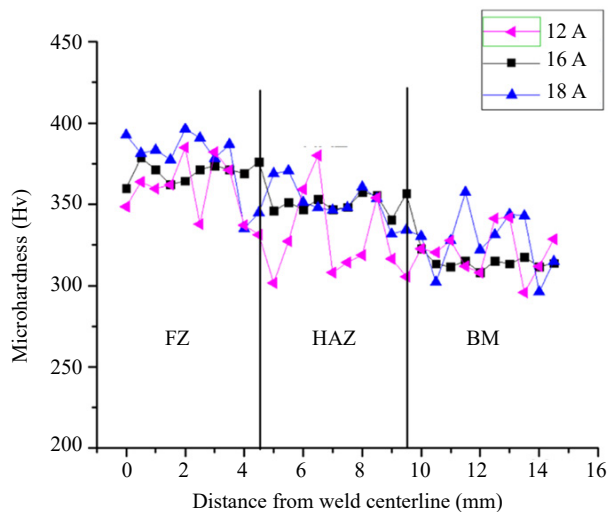


Figure 5. Microhardness distribution at welding currents of 12A, 16 A and 18A

### 3.4 Mechanical properties analysis

The tensile test results of all the weldments, i.e., 12 A, 16 A and 18 A are presented in Table 3. The values of UTS rose as the welding current increased from 12 A to 18 A as shown in Figure 6. This can be attributed to incomplete fusion which led to decreased homogeneity and caused coarseness in the microstructure which decreased the UTS of the weldment at the lower value of current. For higher values of welding current, a higher degree of weld pool agitation allowed homogeneity to increase and caused a refined microstructure which slightly increased the value of UTS.

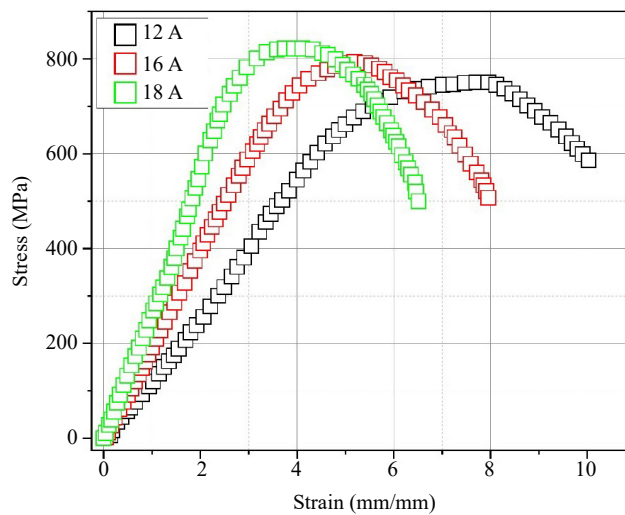


Figure 6. Stress-strain curves of all the specimens (12 A, 16 A and 18 A)

Notched tensile samples were prepared to check the strength of those welded samples which fractured from BM during the smooth tensile test. By increasing the value of the welding current, NTS values also increased gradually as shown in Table 3. Furthermore, it can also be observed by comparing the values of UTS and NTS from Table 3 that the NTS value is always smaller than the UTS value due to the presence of a notch at welded zone which causes stress concentration at the specified notch area. Percentage elongation decreased by increasing the welding current as seen in Table 3. The reduction in percentage elongation may be attributed to an increase in the width of the HAZ. Moreover, impact toughness values increased by increasing the value of welding current which may be attributed to an increase in weld pool penetration which further increased the volume of the welded region below the V-notch impact samples. Thus energy absorbed increased during impact loading as shown in Table 3 [21].

Table 3. Effect of input parameters on welding characteristics

S.No.	Welding current (A)	Penetration	FZ width (mm)	UTS (MPa)	NTS (MPa)	% Elongation	Impact toughness (J)	Fracture zone
1	12	Partial	2.6	754	703	10	2.3	FZ
2	16	Full	3.0	799	736	8	2.8	FZ
3	18	Full	4.3	810	785	6.5	3.3	FZ

In Figure 7, all samples of tensile either they are smooth or notch, fractured from welded zone except two smooth tensile samples of background current of 12A and 18A. This is due to increased ductility and tensile strength of FZ at the maximum difference of peak current and background current as discussed earlier which caused the BM to fracture.

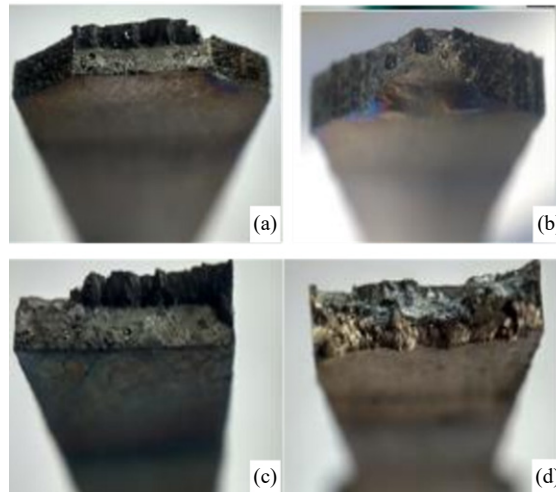


**Figure 7.** Fractured surfaces of all the weldments (a) notch tensile sample at 12 A, (b) notch tensile sample at 18 A, (c) smooth tensile sample at 12 A, and (d) smooth tensile sample at 18 A

## 4. Conclusions

Ti5Sn2.5Al sheets were joined by using pulsed TIG welding at different currents (12 A, 16 A and 18 A) and the following conclusions were drawn:

- The optical microscopy analysis indicated that the 18 A weldment had a relatively higher amount of  $\alpha'$  martensite as compared to the 16 A and 12 A weldment. This could be attributed to the greater cooling rate in 18 A weldment as compared to other weldments which led to  $\alpha'$  martensite formation in its FZ.
- The microhardness measurements were observed to increase in FZ/HAZ by increasing the welding current. The increase in values at FZ/HAZ could be due to a higher amount of  $\alpha'$  martensite transformation in HAZ and FZ.
- Ductility and NTS values were observed to increase with the increase of welding current.

## Conflict of interest

There is no conflict of interest for this study.

## References

- Nie X, Leyland A, Matthews A. Deposition of layered bioceramic hydroxyapatite/TiO<sub>2</sub> coatings on titanium alloys using a hybrid technique of micro-arc oxidation and electrophoresis. *Surface and Coatings Technology*. 2000; 125(1-3): 407-414. [https://doi.org/10.1016/S0257-8972\(99\)00612-X](https://doi.org/10.1016/S0257-8972(99)00612-X)
- Hofmann DC, Suh JY, Wiest A, Lind ML, Demetriou MD, Johnson WL. Development of tough, low-density titanium-based bulk metallic glass matrix composites with tensile ductility. *Proceedings of the National Academy of Sciences*. 2008; 105(51): 20136-20140. <https://doi.org/10.1073/pnas.0809000106>
- Dimiduk DM. Gamma titanium aluminide alloys—an assessment within the competition of aerospace structural materials. *Materials Science and Engineering: A*. 1999; 263(2): 281-288. [https://doi.org/10.1016/S0921-5093\(98\)01158-7](https://doi.org/10.1016/S0921-5093(98)01158-7)
- Karlsson J, Norell M, Ackelid U, Engqvist H, Lausmaa J. Surface oxidation behavior of Ti-6Al-4V manufactured by Electron Beam Melting (EBM®). *Journal of Manufacturing Processes*. 2015; 17: 120-126. <https://doi.org/10.1016/j.jmapro.2014.08.005>
- Kumar C, Das CPM, Paul CP, Singh B. Effect of heat input and defocussing distance on weld quality of laser beam welded titanium alloy. In: *6th International & 27th All India Manufacturing Technology, Design and Research*

Conference, 16-18 December 2016, India.

- [6] Shamir M, Junaid M, Khan FN, Taimoor AA, Baig MN. A comparative study of electrochemical corrosion behavior in Laser and TIG welded Ti-5Al-2.5 Sn alloy. *Journal of Materials Research and Technology*. 2019; 8(1): 87-98. <https://doi.org/10.1016/j.jmrt.2017.09.006>
- [7] Boyer RR. An overview of the use of titanium in the aerospace industry. *Materials Science and Engineering: A*. 1996; 213(1-2): 103-114. [https://doi.org/10.1016/0921-5093\(96\)10233-1](https://doi.org/10.1016/0921-5093(96)10233-1)
- [8] Zhan X, Yan T, Gao Q, Zhu Z, Bu H, Wang Z. The porosity formation mechanism in the laser welded joint of TA15 titanium alloy. *Materials Research Express*. 2019; 6(7): 076558. <https://doi.org/10.1088/2053-1591/AB1612>
- [9] Zhong Y, Xie J, Chen Y, Yin L, He P, Lu W. Microstructure and mechanical properties of micro laser welding NiTiNb/Ti6Al4V dissimilar alloys lap joints with nickel interlayer. *Materials Letters*. 2022; 306: 130896. <https://doi.org/10.1016/j.matlet.2021.130896>
- [10] Junaid M, Khan FN, Mirza MR, Baig MN. Microstructure, mechanical properties and residual stress distribution in pulsed tungsten inert gas welding of Ti-5Al-2.5 Sn alloy. *Proceedings of the Institution of Mechanical Engineers, Part L: Journal of Materials: Design and Applications*. 2019; 233(10): 2030-2044. <https://doi.org/10.1177/1464420718811364>
- [11] Asif H, Khan FN, Shehbaz T, Junaid M, Baig MN. Influence of pulsed Nd: YAG laser welding power on the microstructures and nano creep behaviour of Ti5Al2.5Sn beads. *Proceedings of the Institution of Mechanical Engineers, Part L: Journal of Materials: Design and Applications*. 2023; 237(5): 1159-1171. <https://doi.org/10.1177/14644207221138194>
- [12] Gao XL, Zhang LJ, Liu J, Zhang JX. A comparative study of pulsed Nd: YAG laser welding and TIG welding of thin Ti6Al4V titanium alloy plate. *Materials Science and Engineering: A*. 2013; 559: 14-21. <https://doi.org/10.1016/j.msea.2012.06.016>
- [13] Shehbaz T, Khan FN, Junaid M, Haider J. Investigating the bonding mechanism of P-TIG welded CpTi/Inconel 718 dissimilar joint with Nb interlayer. *Materials Letters*. 2022; 313: 131748. <https://doi.org/10.1016/j.matlet.2022.131748>
- [14] Shehbaz T, Khan FN, Junaid M, Haider J. Investigating nanoindentation creep behavior of pulsed-TIG welded Inconel 718 and commercially pure titanium using a vanadium interlayer. *Metals*. 2021; 11(9): 1492. <https://doi.org/10.3390/met11091492>
- [15] Mehdi B, Badji R, Ji V, Allili B, Bradai D, Deschaux-Beaume F, et al. Microstructure and residual stresses in Ti-6Al-4V alloy pulsed and unpulsed TIG welds. *Journal of Materials Processing Technology*. 2016; 231: 441-448. <https://doi.org/10.1016/j.jmatprotec.2016.01.018>
- [16] Karpagaraj A, Sankaranarayanan K. Some studies on mechanical properties and microstructural characterization of automated TIG welding of thin commercially pure titanium sheets. *Materials Science and Engineering: A*. 2015; 640: 180-189. <https://doi.org/10.1016/j.msea.2015.05.056>
- [17] Tsai CJ, Wang LM. Improved mechanical properties of Ti-6Al-4V alloy by electron beam welding process plus annealing treatments and its microstructural evolution. *Materials & Design*. 2014; 60: 587-598. <https://doi.org/10.1016/J.MATDES.2014.04.037>
- [18] Babu NK, Raman SGS, Mythili R, Saroja S. Correlation of microstructure with mechanical properties of TIG weldments of Ti-6Al-4V made with and without current pulsing. *Materials Characterization*. 2007; 58(7): 581-587. <https://doi.org/10.1016/j.matchar.2006.07.001>
- [19] Balasubramanian V, Jayabalan V, Balasubramanian M. Effect of current pulsing on tensile properties of titanium alloy. *Materials & Design*. 2008; 29(7): 1459-1466. <https://doi.org/10.1016/j.matdes.2007.07.007>
- [20] Akman E, Demir A, Canel T, Sımmazçelik T. Laser welding of Ti6Al4V titanium alloys. *Journal of Materials Processing Technology*. 2009; 209(8): 3705-3713. <https://doi.org/10.1016/j.jmatprotec.2008.08.026>
- [21] Balasubramanian TS, Balakrishnan M, Balasubramanian V, Manickam MM. Influence of welding processes on microstructure, tensile and impact properties of Ti-6Al-4V alloy joints. *Transactions of Nonferrous Metals Society of China*. 2011; 21(6): 1253-1262. [https://doi.org/10.1016/S1003-6326\(11\)60850-9](https://doi.org/10.1016/S1003-6326(11)60850-9)